

MODELING THE EMERGENCE OF PHENOTYPIC HETEROGENEITY IN VASCULARIZED TUMORS*

CHIARA VILLA[†], MARK A. CHAPLAIN[†], AND TOMMASO LORENZI[‡]

Abstract. We present a mathematical study of the emergence of phenotypic heterogeneity in vascularized tumors. Our study is based on formal asymptotic analysis and numerical simulations of a system of nonlocal parabolic equations that describes the phenotypic evolution of tumor cells and their nonlinear dynamic interactions with the oxygen, which is released from the intratumoral vascular network. Numerical simulations are carried out both in the case of arbitrary distributions of intratumor blood vessels and in the case where the intratumoral vascular network is reconstructed from clinical images obtained using dynamic optical coherence tomography. The results obtained support a more in-depth theoretical understanding of the eco-evolutionary process which underpins the emergence of phenotypic heterogeneity in vascularized tumors. In particular, our results offer a theoretical basis for empirical evidence indicating that the phenotypic properties of cancer cells in vascularized tumors vary with the distance from the blood vessels, and establish a relation between the degree of tumor tissue vascularization and the level of intratumor phenotypic heterogeneity.

Key words. nonlocal partial differential equations, mathematical oncology, intratumor heterogeneity, vascularized tumors, eco-evolutionary dynamics

AMS subject classifications. 35Q92, 92C50, 92D25, 35K55

DOI. 10.1137/19M1293971

1. Introduction. Spatial variability in the intratumoral concentration of oxygen plays a pivotal role in the emergence and development of phenotypic heterogeneity among tumor cells [3, 42, 68, 71, 92]. This is exemplified in a growing body of experimental and clinical studies demonstrating that tumor cells with different phenotypic properties occupy tumor regions which are characterized by different oxygen levels. In particular, hypoxic parts of the tumor (i.e., regions where oxygen levels are below normal physiological levels) are mainly populated by slow-dividing cells, which display higher levels of hypoxia-inducible factors, such as HIF-1 [39, 57, 75, 84, 91, 93, 100].

On the other hand, fast-dividing cells with lower levels of expression of hypoxia-inducible factors are primarily detected in well-oxygenated parts of the tumor tissue (i.e., the tumor border in avascular tumors and the regions in the vicinity of blood vessels in vascularized tumors) [39, 93, 84]. This impinges on anti-cancer treatment by making it impossible for single biopsies to exhaustively portray the phenotypic composition of the whole tumor tissue [18, 78, 99].

Previous empirical and theoretical work has suggested that this may be the outcome of eco-evolutionary dynamics driven by interactions between oxygen molecules and tumor cells [3, 35, 38, 62, 68, 69]. In particular, it has been hypothesized that the nonlinear interplay between impaired oxygen delivery caused by structural abnormalities present in the tumor vasculature [34, 51, 52, 75, 95], limited oxygen diffusion and oxygen consumption by tumor cells may lead to the creation of distinct

*Received by the editors October 17, 2019; accepted for publication (in revised form) January 13, 2021; published electronically March 30, 2021.

<https://doi.org/10.1137/19M1293971>

[†]School of Mathematics and Statistics, University of St. Andrews, St. Andrews, Fife, KY16 9SS, Scotland (cv23@st-andrews.ac.uk, majc@st-andrews.ac.uk).

[‡]Department of Mathematical Sciences, Politecnico di Torino, Torino, 10129, Italy (tommaso.lorenzi@polito.it).

ecological niches in which tumor cells with different phenotypic characteristics can be selected [3, 20, 36, 46, 49, 61].

In this paper, we use a spatially explicit phenotype-structured model to elucidate the eco-evolutionary dynamics that underpin the emergence of phenotypic heterogeneity in vascularized tumors. Building upon the modeling framework that we developed in [64, 65], the model comprises a nonlocal parabolic partial differential equation (PDE) that governs the local phenotypic distribution of cells within the tumor tissue. Similar PDEs modeling the evolutionary dynamics of space- and phenotype-structured populations have recently received increasing attention from the mathematical community—see, for instance, [1, 2, 10, 13, 14, 15, 19, 28, 47, 50, 70].

The equation for the evolution of the local phenotypic distribution of tumor cells is coupled with a parabolic PDE that governs the local concentration of oxygen, whereby a spatially heterogeneous source term captures the presence of intratumoral blood vessels which bring oxygen into the tumor tissue. Different possible definitions of such a source term are considered, including definitions that are derived from clinical images obtained using dynamic optical coherence tomography (D-OCT) [82]—i.e., a noninvasive imaging technique that enables the visualization of cutaneous microvasculature in 2D tissue sections with a width of and at a depth of up to several millimeters [73].

Compared to previous related studies [64, 65], our model takes into account the effect of movement and phenotypic variation of tumor cells and, in addition, it does not rely on a quasi-stationary equilibrium assumption for the oxygen concentration. Furthermore, while these previous studies are mainly focused on avascular tumors, in this paper we consider vascularized tumors and systematically assess the impact of the degree of tumor tissue vascularization on the level of phenotypic heterogeneity of tumor cells, which is mathematically quantified through suitable diversity indices. Moreover, numerical solutions of the model equations are here integrated with the results of formal asymptotic analysis in order to achieve more robust and precise biological conclusions. Taken together, these elements of novelty widen considerably the range of application of the results of our study and support a more in-depth theoretical understanding of the eco-evolutionary process which leads to the emergence of phenotypic heterogeneity in vascularized tumors.

The paper is organized as follows. In section 2, we introduce the equations of the model and the underlying modeling assumptions. In section 3, we carry out a formal asymptotic analysis of evolutionary dynamics. In section 4, we present a sample of numerical solutions that confirm the results of our formal analysis, and we discuss their biological implications. Section 5 concludes the paper and provides a brief overview of possible research perspectives.

2. Description of the model. We model the evolutionary dynamics of cancer cells in a region of a vascularized tumor, which is approximated as a bounded set $\Omega \subset \mathbb{R}^d$ with smooth boundary $\partial\Omega$, where $d = 1, 2, 3$ depending on the biological scenario under study. The spatial position of the tumor cells is described by a vector $\mathbf{r} \in \Omega$, while the phenotypic state of the cells is modeled by a scalar variable $x \in [0, 1] \subset \mathbb{R}$, which represents the normalized level of expression of a hypoxia-inducible factor. The phenotypic distribution of tumor cells at time $t \geq 0$ and position \mathbf{r} is described by the function $n(t, \mathbf{r}, x)$, while the function $s(t, \mathbf{r})$ describes the oxygen concentration at time t and position \mathbf{r} .

At each time t , we define the local cell density and the local mean phenotypic state of tumor cells, respectively, as

$$(2.1) \quad I(t, \mathbf{r}) := \int_0^1 n(t, \mathbf{r}, x) dx \quad \text{and} \quad X(t, \mathbf{r}) := \frac{1}{I(t, \mathbf{r})} \int_0^1 x n(t, \mathbf{r}, x) dx.$$

Moreover, we define the total cell number and the fraction of cells in the phenotypic state x within the tumor, respectively, as

$$(2.2) \quad N(t) := \int_{\Omega} I(t, \mathbf{r}) d\mathbf{r} \quad \text{and} \quad F(t, x) := \frac{1}{N(t)} \int_{\Omega} n(t, \mathbf{r}, x) d\mathbf{r}.$$

2.1. Dynamic of tumor cells. Tumor cells divide, die, move randomly (i.e., undergo undirected, spontaneous migration) and undergo spontaneous epimutations, that is, heritable phenotypic changes that occur randomly due to nongenetic instability and are not induced by any selective pressure [48]. The dynamic of the local cell phenotypic distribution $n(t, \mathbf{r}, x)$ is governed by the following boundary value problem subject to a suitable initial condition:

$$(2.3) \quad \begin{cases} \partial_t n = \underbrace{R(x, I(t, \mathbf{r}), s(t, \mathbf{r}))n}_{\text{cell division and death}} + \underbrace{\alpha \partial_{xx}^2 n}_{\text{spontaneous epimutations}} + \underbrace{\beta \Delta_{\mathbf{r}} n}_{\text{random movement}} & \text{in } \Omega \times (0, 1), \\ I(t, \mathbf{r}) := \int_0^1 n(t, \mathbf{r}, x) dx, \\ \partial_x n(\cdot, \cdot, 0) = \partial_x n(\cdot, \cdot, 1) = 0, \\ \nabla_{\mathbf{r}} n \cdot \hat{\mathbf{u}} = 0 \quad \text{on } \partial\Omega, \end{cases}$$

where $\hat{\mathbf{u}}$ is the unit normal to $\partial\Omega$ that points outward from Ω .

The first diffusion term on the right-hand side of the nonlocal parabolic equation (2.3)₁ describes the effect of changes in the local phenotypic distribution due to spontaneous epimutations, which occur at rate α [23, 63]. The second diffusion term models the effect of cell random movement and the parameter β represents the cell motility. The function $R(x, I(t, \mathbf{r}), s(t, \mathbf{r}))$ models the fitness of tumor cells in the phenotypic state x at position \mathbf{r} and time t under the local environmental conditions given by the cell density $I(t, \mathbf{r})$ and the oxygen concentration $s(t, \mathbf{r})$ (i.e., the phenotypic fitness landscape of the tumor). In particular, we define the function R as

$$(2.4) \quad R(x, I, s) := p(x, s) - \kappa I.$$

Definition (2.4) models a biological scenario whereby tumor cells die at position \mathbf{r} and time t due to competition for limited space at rate $\kappa I(t, \mathbf{r})$, with the parameter κ being related to the local carrying capacity of the tumor. Moreover, the function $p(x, s(t, \mathbf{r}))$ is the division rate of cells in the phenotypic state x at position \mathbf{r} and time t under the oxygen concentration $s(t, \mathbf{r})$. Building upon the modeling strategy presented in [64], we define the cell division rate as

$$(2.5) \quad p(x, s) := f(x) + g(x, s).$$

In (2.5), the function $g(x, s(t, \mathbf{r}))$ represents the rate of cell division via aerobic pathways under the oxygen concentration $s(t, \mathbf{r})$, while the function $f(x)$ models the rate of cell division via anaerobic pathways. Based on the biological evidence and ideas presented in [3, 8, 43, 61, 98], we let cells with a lower level of expression of the hypoxia-inducible factor (i.e., cells in phenotypic states $x \rightarrow 0$) be characterized by a higher

rate of cell division via aerobic pathways, while we assume cells with a higher level of expression of the hypoxia-inducible factor (i.e., cells in phenotypic states $x \rightarrow 1$) to be characterized by a higher rate of cell division via anaerobic pathways. Therefore, we assume the functions $f(x)$ and $g(x, s)$ to be smooth and such that

$$(2.6) \quad f(0) = 0, \quad f'(x) > 0 \quad \forall x \in [0, 1],$$

$$(2.7) \quad g(1, s) = 0 \quad \forall s \in [0, \infty), \quad \partial_x g(x, s) < 0 \quad \forall (x, s) \in (0, 1] \times (0, \infty).$$

Moreover, we make the following natural assumptions

$$(2.8) \quad g(x, 0) = 0 \quad \forall x \in [0, 1], \quad \partial_s g(x, s) > 0 \quad \forall (x, s) \in [0, 1] \times (0, \infty).$$

2.2. Dynamic of oxygen. We let oxygen enter the tumor through intratumoral blood vessels, diffuse in space, decay over time and be consumed by tumor cells which divide via aerobic pathways. In this scenario, the dynamic of the oxygen concentration $s(t, \mathbf{r})$ is governed by the following boundary value problem:

$$(2.9) \quad \begin{cases} \partial_t s = \underbrace{\beta_s \Delta_{\mathbf{r}} s}_{\text{diffusion}} - \underbrace{\eta_s \int_0^1 g(x, s) n(t, \mathbf{r}, x) dx}_{\text{consumption by tumor cells}} - \underbrace{\lambda_s s}_{\text{decay}} + \underbrace{q(t, \mathbf{r})}_{\text{inflow from blood vessels}} & \text{in } \Omega, \\ \nabla_{\mathbf{r}} s \cdot \hat{\mathbf{u}} = 0 & \text{on } \partial\Omega, \end{cases}$$

subject to a suitable initial condition and coupled to the nonlocal parabolic equation (2.3)₁.

In the parabolic equation (2.9)₁, the parameter β_s is the oxygen diffusion coefficient, η_s is a conversion factor linked to the rate of oxygen consumption by tumor cells, λ_s is the natural decay rate of oxygen, and the source term $q(t, \mathbf{r})$ models the influx of oxygen from the intratumoral blood vessels. We let $\omega \subset \Omega$ be the set of points within the tumor tissue which are occupied by blood vessels and, since we do not consider the formation of new blood vessels, we assume ω to be given and remain constant in time. Therefore, we use the following definition

$$(2.10) \quad q(t, \mathbf{r}) := S(t, \mathbf{r}) \mathbf{1}_\omega(\mathbf{r}),$$

where $\mathbf{1}_\omega$ is the indicator function of the set ω and $S(t, \mathbf{r})$ is the rate of inflow of oxygen through intratumoral blood vessels at position $\mathbf{r} \in \omega$ and time t .

Remark 2.1. In this paper, we do not take into account the effect of mechanical interactions between tumor cells and blood vessels and we do not allow tumor cell to extravasate. Therefore, focusing on the case of intratumoral blood vessels of small size, we implicitly make the following simplifying assumptions: (i) a point \mathbf{r} can be simultaneously occupied by blood vessels and tumor cells; (ii) cell movement is not affected by the presence of blood vessels. Therefore, we do not impose any condition on $n(t, \mathbf{r}, x)$ in ω .

3. Formal analysis of evolutionary dynamics. In order to obtain an analytical description of the evolutionary dynamics of tumor cells, in this section we carry out a formal asymptotic analysis of the behavior of the solution to the problem given by (2.3) subject to a suitable initial condition, under the assumption

$$(3.1) \quad s(t, \mathbf{r}) \equiv s^\infty(\mathbf{r}),$$

where $s^\infty(\mathbf{r})$ is a given smooth positive function. We note that assumptions (2.6)–(2.8) ensure that

$$(3.2) \quad 0 < p(x, s) < \infty \quad \forall (x, s) \in [0, 1] \times (0, \infty).$$

Moreover, focusing on an intratumor phenotypic fitness landscape $R(x, I, s^\infty)$ defined according to (2.4) with a single peak at each position \mathbf{r} and time t , we let the cell division rate p be a smooth function that satisfies the additional concavity assumption

$$(3.3) \quad \partial_{xx}^2 p(x, s) < 0 \quad \forall (x, s) \in [0, 1] \times (0, \infty).$$

Typical values of the epimutation rate α are one or two orders of magnitude larger than the rate of somatic DNA mutation [27, p. 45], which is about 10^{-12} s^{-1} [29], and typical values of the cell diffusivity β are about $10^{-12} \text{ cm}^2 \text{ s}^{-1}$ [88, 96]. Hence, spontaneous epimutations and random cell movement occur on slower time scales compared to cell division and death. To capture this fact, we introduce a small parameter $\varepsilon > 0$ and assume both $\alpha := \varepsilon^2$ and $\beta := \varepsilon^2$.

Following previous studies on the long-time behavior of nonlocal PDEs and integrodifferential equations modeling the dynamics of continuously structured populations [12, 22, 25, 26, 50, 66, 70, 77], we use the time scaling $t \mapsto \frac{t}{\varepsilon}$ in the balance equation (2.3)₁ complemented with (3.1), which gives the following nonlocal PDE for the local cell phenotypic distribution $n(\frac{t}{\varepsilon}, \mathbf{r}, x) = n_\varepsilon(t, \mathbf{r}, x)$

$$(3.4) \quad \varepsilon \partial_t n_\varepsilon = R(x, I_\varepsilon(t, \mathbf{r}), s^\infty(\mathbf{r})) n_\varepsilon + \varepsilon^2 \partial_{xx}^2 n_\varepsilon + \varepsilon^2 \Delta_{\mathbf{r}} n_\varepsilon.$$

Considering the asymptotic regime $\varepsilon \rightarrow 0$ is equivalent to studying the behavior of $n_\varepsilon(t, \mathbf{r}, x)$ over many cell generations and in the case where spontaneous epimutations and random cell movement induce small changes in the local phenotypic distribution.

Moreover, in agreement with much of the previous work on the mathematical analysis of the evolutionary dynamics of continuously structured populations [76], we consider the case where at time $t = 0$ tumor cells that occupy the same position are mainly in the same phenotypic state; that is, at every position \mathbf{r} the initial local cell phenotypic distribution $n_\varepsilon(0, \mathbf{r}, x)$ is a sharp Gaussian-like function with mean value $\bar{x}^0(\mathbf{r})$ and integral $I_\varepsilon(0, \mathbf{r})$. Hence, we assume

$$(3.5) \quad n_\varepsilon(0, \mathbf{r}, x) = e^{u_\varepsilon^0(\mathbf{r}, x)/\varepsilon}$$

with $u_\varepsilon^0(\mathbf{r}, x)$ being a smooth, uniformly concave function of x for every $\mathbf{r} \in \Omega$ such that

$$(3.6) \quad 0 < I_\varepsilon(0, \mathbf{r}) < \infty$$

and

$$(3.7) \quad e^{u_\varepsilon^0(\mathbf{r}, x)/\varepsilon} \xrightarrow[\varepsilon \rightarrow 0]{*} I(0, \mathbf{r}) \delta_{\bar{x}^0(\mathbf{r})}(x) \quad \forall \mathbf{r} \in \Omega$$

in the sense of measures, where $\delta_{\bar{x}^0(\mathbf{r})}(x)$ is the Dirac delta distribution centered at $\bar{x}^0(\mathbf{r})$.

Building upon the method presented in [12, 26, 66, 76, 77], we make the real phase WKB (Wentzel–Kramers–Brillouin) ansatz [11, 30, 32]

$$(3.8) \quad n_\varepsilon(t, \mathbf{r}, x) = e^{u_\varepsilon(t, \mathbf{r}, x)/\varepsilon}.$$

Substituting this ansatz into (3.4) and using

$$\begin{aligned}\partial_t n_\varepsilon &= \varepsilon^{-1} n_\varepsilon \partial_t u_\varepsilon, \quad \nabla_{\mathbf{r}} n_\varepsilon = \varepsilon^{-1} n_\varepsilon \nabla_{\mathbf{r}} u_\varepsilon, \quad \partial_x n_\varepsilon = \varepsilon^{-1} n_\varepsilon \partial_x u_\varepsilon, \\ \Delta_{\mathbf{r}} n_\varepsilon &= \left(\varepsilon^{-1} |\nabla_{\mathbf{r}} u_\varepsilon| \right)^2 n_\varepsilon + \varepsilon^{-1} n_\varepsilon \Delta_{\mathbf{r}} u_\varepsilon, \quad \partial_{xx}^2 n_\varepsilon = \left(\varepsilon^{-1} \partial_x u_\varepsilon \right)^2 n_\varepsilon + \varepsilon^{-1} n_\varepsilon \partial_{xx}^2 u_\varepsilon,\end{aligned}$$

we obtain

$$(3.9) \quad \partial_t u_\varepsilon = R(x, I_\varepsilon(t, \mathbf{r}), s^\infty(\mathbf{r})) + (\partial_x u_\varepsilon)^2 + |\nabla_{\mathbf{r}} u_\varepsilon|^2 + \varepsilon (\partial_{xx}^2 u_\varepsilon + \Delta_{\mathbf{r}} u_\varepsilon)$$

subject to the initial condition $u_\varepsilon(0, \mathbf{r}, x) = u_\varepsilon^0(\mathbf{r}, x)$, with $u_\varepsilon^0(\mathbf{r}, x)$ given by (3.5).

Letting $\varepsilon \rightarrow 0$ in (3.9) we formally obtain the following equation for the leading-order term u of the asymptotic expansion for u_ε :

$$(3.10) \quad \partial_t u = R(x, I(t, \mathbf{r}), s^\infty(\mathbf{r})) + (\partial_x u)^2 + |\nabla_{\mathbf{r}} u|^2 \quad \text{in } \Omega \times (0, 1),$$

where $I(t, \mathbf{r})$ is the leading-order term of the asymptotic expansion for $I_\varepsilon(t, \mathbf{r})$.

Since u_ε^0 is a uniformly concave function of x and, under assumption (3.3), R is a concave function of x as well, we expect u to be a concave function of x [12, 70, 77]. Therefore, we formally have that there exists a unique locally dominant phenotypic state $\bar{x}(t, \mathbf{r})$, which is such that $u(t, \mathbf{r}, \bar{x}(t, \mathbf{r})) = \max_{x \in [0, 1]} u(t, \mathbf{r}, x)$ and

$$(3.11) \quad \partial_x u(t, \mathbf{r}, \bar{x}(t, \mathbf{r})) = 0.$$

Moreover, (3.2) and (3.6) ensure that $0 < I_\varepsilon(t, \mathbf{r}) < \infty$ and, therefore, letting $\varepsilon \rightarrow 0$ in (3.8) gives the constraint

$$(3.12) \quad u(t, \mathbf{r}, \bar{x}(t, \mathbf{r})) = 0 \quad \forall (t, \mathbf{r}) \in (0, \infty) \times \Omega.$$

Evaluating (3.10) at $x = \bar{x}(t, \mathbf{r})$ and using (3.11) along with (3.12) yields

$$(3.13) \quad R(\bar{x}(t, \mathbf{r}), I(t, \mathbf{r}), s^\infty(\mathbf{r})) = 0.$$

Differentiating (3.11) with respect to t yields

$$\partial_{tx} u(t, \mathbf{r}, \bar{x}(t, \mathbf{r})) + \partial_{xx}^2 u(t, \mathbf{r}, \bar{x}(t, \mathbf{r})) \partial_t \bar{x}(t, \mathbf{r}) = 0,$$

and, using the fact that $\partial_{xx}^2 u(t, \mathbf{r}, \bar{x}(t, \mathbf{r})) < 0$, we can formally rewrite the above equation as

$$(3.14) \quad \partial_t \bar{x}(t, \mathbf{r}) = -(\partial_{xx}^2 u(t, \mathbf{r}, \bar{x}(t, \mathbf{r})))^{-1} \partial_{tx} u(t, \mathbf{r}, \bar{x}(t, \mathbf{r})).$$

Furthermore, differentiating both sides of (3.10) with respect to x , evaluating the resulting equation at $x = \bar{x}(t, \mathbf{r})$, and using (3.11) along with (3.12) gives

$$\partial_{tx} u(t, \mathbf{r}, \bar{x}(t, \mathbf{r})) = \partial_x R(\bar{x}(t, \mathbf{r}), I(t, \mathbf{r}), s^\infty(\mathbf{r})).$$

Substituting the latter equation into (3.14) we formally obtain the following equation for $\bar{x}(t, \mathbf{r})$:

$$(3.15) \quad \partial_t \bar{x}(t, \mathbf{r}) = -(\partial_{xx}^2 u(t, \mathbf{r}, \bar{x}(t, \mathbf{r})))^{-1} \partial_x R(\bar{x}(t, \mathbf{r}), I(t, \mathbf{r}), s^\infty(\mathbf{r})).$$

Combining (3.13) and (3.15) we find that the steady-state values of $I(t, \mathbf{r})$ and $\bar{x}(t, \mathbf{r})$, say, $I^\infty(\mathbf{r})$ and $\bar{x}^\infty(\mathbf{r})$, need to satisfy

$$\begin{cases} R(\bar{x}^\infty(\mathbf{r}), I^\infty(\mathbf{r}), s^\infty(\mathbf{r})) = 0, \\ \partial_x R(\bar{x}^\infty(\mathbf{r}), I^\infty(\mathbf{r}), s^\infty(\mathbf{r})) = 0. \end{cases}$$

Substituting (2.4) into the above system of equations, we formally obtain

$$(3.16) \quad \begin{cases} p(\bar{x}^\infty(\mathbf{r}), s^\infty(\mathbf{r})) - \kappa I^\infty(\mathbf{r}) = 0, \\ \partial_x p(\bar{x}^\infty(\mathbf{r}), s^\infty(\mathbf{r})) = 0, \end{cases} \implies \begin{cases} I^\infty(\mathbf{r}) = \frac{1}{\kappa} p(\bar{x}^\infty(\mathbf{r}), s^\infty(\mathbf{r})), \\ \bar{x}^\infty(\mathbf{r}) = \arg \max_{x \in [0,1]} p(x, s^\infty(\mathbf{r})). \end{cases}$$

Taken together, these formal results indicate that, in the framework of the assumptions considered in this section, we can expect the local cell phenotypic distribution at steady-state $n^\infty(\mathbf{r}, x)$ to be of the form

$$(3.17) \quad n^\infty(\mathbf{r}, x) = I^\infty(\mathbf{r}) \delta_{\bar{x}^\infty(\mathbf{r})}(x),$$

with the local cell density $I^\infty(\mathbf{r})$ and the locally dominant phenotypic state $\bar{x}^\infty(\mathbf{r})$ both given by (3.16). This also implies that the local mean phenotypic state of the tumor cells at steady-state, say, $X^\infty(\mathbf{r})$, coincides with $\bar{x}^\infty(\mathbf{r})$, that is,

$$X^\infty(\mathbf{r}) := \frac{1}{I^\infty(\mathbf{r})} \int_0^1 x n^\infty(\mathbf{r}, x) dx = \bar{x}^\infty(\mathbf{r}).$$

4. Numerical solutions. In this section, we construct numerical solutions to the problem given by (2.3) and (2.9) subject to suitable initial conditions. First, we describe the setup of numerical simulations and the model parameterization (see section 4.1). Then, we present a sample of numerical solutions that confirm the results of the formal analysis of evolutionary dynamics carried out in section 3. We consider both the case of an arbitrary distribution of blood vessels (see section 4.2) and the case where the blood vessel distribution is reconstructed from clinical images obtained via D-OCT (section 4.3). Finally, we use numerical solutions of the model equations to assess the impact of tumor tissue vascularization on intratumor phenotypic heterogeneity (see section 4.4).

4.1. Setup of numerical simulations and model parameterization. Building upon the modeling strategy presented in [64], we define the functions $f(x)$ and $g(x, s)$ that compose the cell division rate $p(x, s)$ as

$$(4.1) \quad f(x) := \varphi \left[1 - (1 - x)^2 \right] \quad \text{and} \quad g(x, s) := \gamma \frac{s}{\mu + s} (1 - x^2), \quad \varphi < \gamma.$$

In (4.1), the parameters $\varphi > 0$ and $\gamma > 0$ model the maximum rate of cell division via anaerobic and aerobic pathways, respectively, while $\mu > 0$ is the Michaelis–Menten constant of oxygen. The assumption $\varphi < \gamma$ is based on empirical evidence indicating that higher levels of expression of hypoxia-inducible factors correlate with lower rates of cell division [16, 17, 61]. Definitions (4.1) satisfy the general assumptions (2.6)–(2.8) and (3.3) and allow for a detailed quantitative characterization of the evolutionary dynamics of tumor cells based on the formal results presented in section 3. Moreover, they lead to a phenotypic fitness landscape of the tumor $R(x, I, s)$ that is close to the

approximate fitness landscapes which can be inferred from experimental data through regression techniques [55, 74, 90]. In fact, substituting (4.1) into (2.5), after a little algebra we find

$$(4.2) \quad p(x, s) = a(s) - b(s)(x - h(s))^2,$$

where

$$(4.3) \quad a(s) := \gamma \frac{s}{\mu + s} + \frac{\varphi^2}{\varphi + \gamma \frac{s}{\mu + s}}, \quad b(s) := \varphi + \gamma \frac{s}{\mu + s}, \quad h(s) := \frac{\varphi}{\varphi + \gamma \frac{s}{\mu + s}}.$$

Here, $a(s(t, \mathbf{r}))$ is the maximum fitness, $h(s(t, \mathbf{r}))$ is the fittest phenotypic state, and $b(s(t, \mathbf{r}))$ is a nonlinear selection gradient at position \mathbf{r} and time t under the environmental conditions corresponding to the oxygen concentration $s(t, \mathbf{r})$.

We let the rate of inflow of oxygen through intratumor blood vessels to be constant in time and the same for all vessels; i.e., we define the function $S(t, \mathbf{r})$ in (2.10) as

$$(4.4) \quad S(t, \mathbf{r}) \equiv S_v > 0.$$

Moreover, we consider different definitions of the set ω which represent different distributions of the blood vessels, as detailed in the next subsections. Unless otherwise explicitly stated, numerical simulations are carried out using the parameter values listed in Table 1, which are chosen to be consistent with the existing literature.

We define $\Omega := [0, L] \times [0, L]$ and choose $L = 0.5$. Under the parameter choice of Table 1, this value of L is equivalent to considering a square region of a 2D cross-section of a vascularized tumor of area $2.5 \times 10^{-3} \text{ cm}^2$. Moreover, we assume $t \in [0, T]$, with the final time T such that the numerical solutions are sufficiently close to equilibrium at the end of simulations. Finally, we use the notation $\mathbf{r} \equiv (r_1, r_2)$.

We complement (2.3) and (2.9) with the following initial conditions:

$$(4.5) \quad n(0, \mathbf{r}, x) = 10^8 e^{-\frac{(x-0.5)^2}{0.1}} \quad \forall \mathbf{r} \in \Omega \quad \text{and} \quad s(0, \mathbf{r}) = S_0 \mathbf{1}_\omega(\mathbf{r}),$$

where $S_0 = 6.3996 \times 10^{-7} \text{ g cm}^{-2}$ [54]. The initial conditions (4.5) correspond to a biological scenario whereby at time $t = 0$ tumor cells are uniformly distributed across Ω and are mainly in the intermediate phenotypic state $x = 0.5$, while the oxygen is concentrated in correspondence of the blood vessels.

TABLE 1
Parameter values used in numerical simulations.

Parameter	Biological meaning	Value	Reference
μ	Michaelis–Menten constant of oxygen	$1.5 \times 10^{-7} \text{ g cm}^{-2}$	[20]
β	Cell motility	$10^{-13} \text{ cm}^2 \text{ s}^{-1}$	[88, 96]
β_s	Oxygen diffusivity	$2 \times 10^{-5} \text{ cm}^2 \text{ s}^{-1}$	[45]
γ	Maximum rate of cell division via aerobic pathways	$1 \times 10^{-4} \text{ s}^{-1}$	[20, 97]
κ	Rate of cell death due to competition for space	$2 \times 10^{-13} \text{ cm}^2 \text{ s}^{-1} \text{ cells}^{-1}$	[59, 64]
η_s	Conversion factor for cell consumption of oxygen	$2 \times 10^{-11} \text{ g cells}^{-1}$	[20, 64]
α	Rate of spontaneous phenotypic changes	10^{-13} s^{-1}	[27, 29]
λ_s	Rate of natural decay of oxygen	$2.78 \times 10^{-6} \text{ s}^{-1}$	[24]
φ	Maximum rate of cell division via anaerobic pathways	$1 \times 10^{-5} \text{ s}^{-1}$	[43]
S_v	Constant rate of inflow of oxygen through blood vessels	$6.3996 \times 10^{-7} \text{ g cm}^{-2} \text{ s}^{-1}$	[54]

Numerical solutions are constructed using a uniform discretization of the square $[0, L] \times [0, L]$ as the computational domain of the independent variable \mathbf{r} and a uniform discretization of the set $[0, 1]$ as the computational domain of the independent variable x . We also discretize the interval $[0, T]$ with a uniform step. The method for constructing numerical solutions is based on an explicit finite difference scheme in which three-point and five-point stencils are used to approximate the diffusion terms in x and \mathbf{r} , respectively, and an explicit finite difference scheme is used for the reaction terms [58]. All numerical computations are performed in MATLAB.

4.2. Numerical solutions for arbitrary blood vessel distributions. Substituting (4.2) into (3.16) gives the following expressions for the local cell density and the locally dominant phenotypic state at steady-state

$$(4.6) \quad I^\infty(\mathbf{r}) \equiv I^\infty(s^\infty(\mathbf{r})) = \frac{a(s^\infty(\mathbf{r}))}{\kappa} \quad \text{and} \quad \bar{x}^\infty(\mathbf{r}) \equiv \bar{x}^\infty(s^\infty(\mathbf{r})) = h(s^\infty(\mathbf{r})),$$

where $a(s^\infty)$ and $h(s^\infty)$ are the maximum fitness and the fittest phenotypic state defined according to (4.3).

In agreement with the results of the formal analysis of evolutionary dynamics carried out in section 3 (cf. the expression (3.17) of the local cell phenotypic distribution at steady-state), the numerical results displayed in Figure 1 show that the cell density $I(T, \mathbf{r})$ and the mean phenotypic state $X(T, \mathbf{r})$, which are computed using the numerical solution $n(T, \mathbf{r}, x)$ of (2.3), coincide with $I^\infty(\mathbf{r})$ and $\bar{x}^\infty(\mathbf{r})$, which are computed through (4.6) choosing $s^\infty(\mathbf{r}) = s(T, \mathbf{r}, x)$, where $s(T, \mathbf{r}, x)$ is the numerical solution of (2.9). Moreover, the numerical solution $n(T, \mathbf{r}, x)$ is concentrated as a sharp Gaussian-like function (data not shown) with maximum at the mean phenotypic state $X(T, \mathbf{r})$ (vid. insets in the fourth panels of Figure 1).

The numerical results of Figure 1, which refer to the blood vessel distribution displayed in the first panel of the figure, indicate that the oxygen concentration is maximal in the vicinity of the blood vessels and decreases monotonically with the distance from the blood vessels. Accordingly, the cell density is higher in the regions in close proximity to the blood vessels and the mean phenotypic state increases from values close to $x = 0$ (i.e., low levels of expression of the hypoxia-inducible factor) to values close to $x = 1$ (i.e., high levels of expression of the hypoxia-inducible factor) moving away from the blood vessels. These results communicate the biological notion that spatial inhomogeneities in the distribution of oxygen—which emerge spontaneously as a result of the nonlinear interplay between the spatial distribution of the blood vessels, the reaction-diffusion dynamics of the oxygen, and the consumption of oxygen by the cells—create environmental conditions that favor the selection of cells with different phenotypic characteristics in different regions of vascularized tumors, thus leading to the emergence and development of intratumor phenotypic heterogeneity.

4.3. Numerical solutions for blood vessel distributions reconstructed from clinical images. The plots in Figure 2 demonstrate that the qualitative behavior of the numerical results in Figure 1 remains unchanged when spatial distributions of the intratumor blood vessels reconstructed from clinical images are considered. These are the plots of the oxygen concentration $s(T, \mathbf{r})$, the cell density $I(T, \mathbf{r})$, and the mean phenotypic state $X(T, \mathbf{r})$ obtained by solving numerically the problem given by (2.3) and (2.9) subject to the initial conditions (4.5), with ω defined according to the distributions of blood vessels provided by the clinical images displayed in the first column of the figure, which were obtained via D-OCT and correspond to three cross

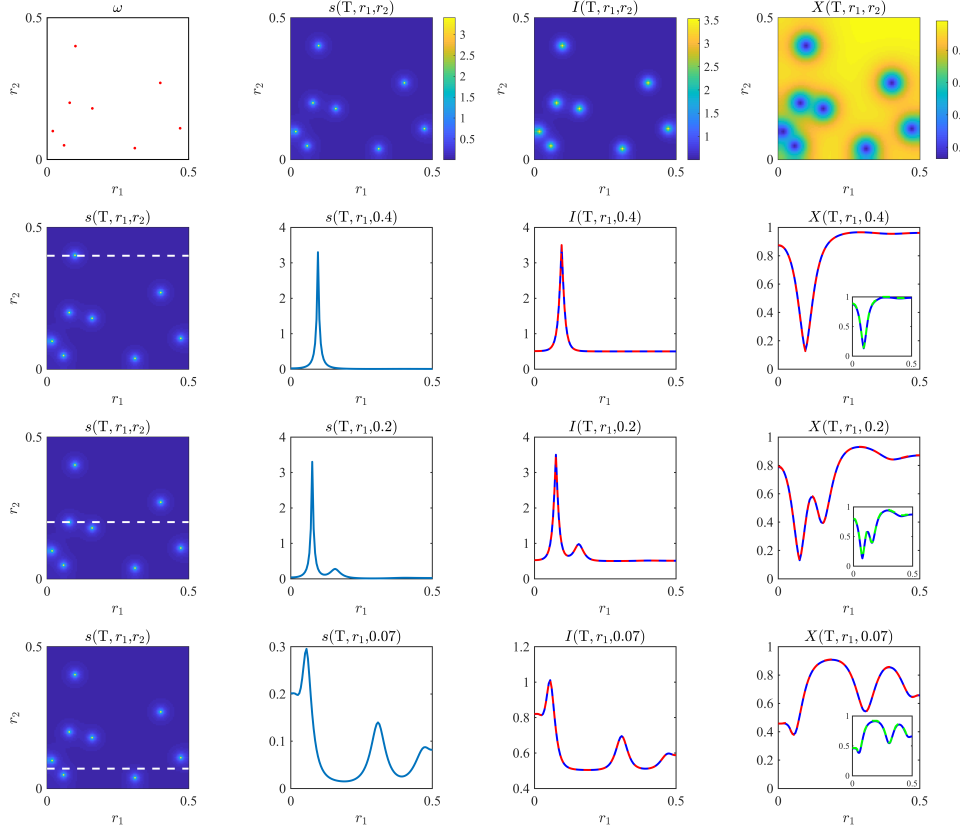


FIG. 1. First row. Plots of the oxygen concentration $s(T, \mathbf{r})$ (second panel), the cell density $I(T, \mathbf{r})$ (third panel), and the mean phenotypic state $X(T, \mathbf{r})$ (fourth panel) obtained by solving numerically the problem given by (2.3) and (2.9) subject to the initial conditions (4.5), with the set ω corresponding to the parts of Ω highlighted in red in the first panel and with the parameter values listed in Table 1. Second row. Plots of the oxygen concentration $s(T, r_1, 0.4)$ (second panel), the cell density $I(T, r_1, 0.4)$ (third panel, blue line), and the mean phenotypic state $X(T, r_1, 0.4)$ (fourth panel, blue line). The plot of the oxygen distribution $s(T, \mathbf{r})$ is displayed in the first panel, where the white, dashed line highlights the 1D cross-section corresponding to $r_2 = 0.4$. The red lines in the third and fourth panels highlight $I^\infty(\mathbf{r})$ and $\bar{x}^\infty(\mathbf{r})$ computed through (4.6) choosing $s^\infty(\mathbf{r}) = s(T, \mathbf{r}, x)$. The inset in the fourth panel displays the plot of the mean phenotypic state $X(T, r_1, 0.4)$ (blue line) and of the maximum point of $n(T, r_1, 0.4, x)$ (green line). Third and fourth rows. Same as the second row but for $r_2 = 0.2$ (third row) and $r_2 = 0.07$ (fourth row). The oxygen concentration $s(T, \mathbf{r})$ is in units of $10^{-7} \text{ g cm}^{-2}$, the cell density $I(T, \mathbf{r})$ is in units of $10^8 \text{ cells cm}^{-2}$, and the spatial variables r_1 and r_2 are in units of cm.

sections of a malignant melanoma at a depth of 0.02 cm (top panel), 0.03 cm (central panel) and 0.04 cm (bottom panel) from the surface of the epidermis [82, Fig. 5].

These results also indicate that increasing levels of tumor vascularization (from top to bottom panel in the first column) lead to a more homogeneous spatial distribution of oxygen (second column), which correlates with a more uniform cell density (third column) and a less diverse mean phenotypic state (fourth column). This suggests the existence of a relationship between the level of tumor tissue vascularization and the level of intratumor phenotypic heterogeneity, which is systematically investigated in the next subsection.

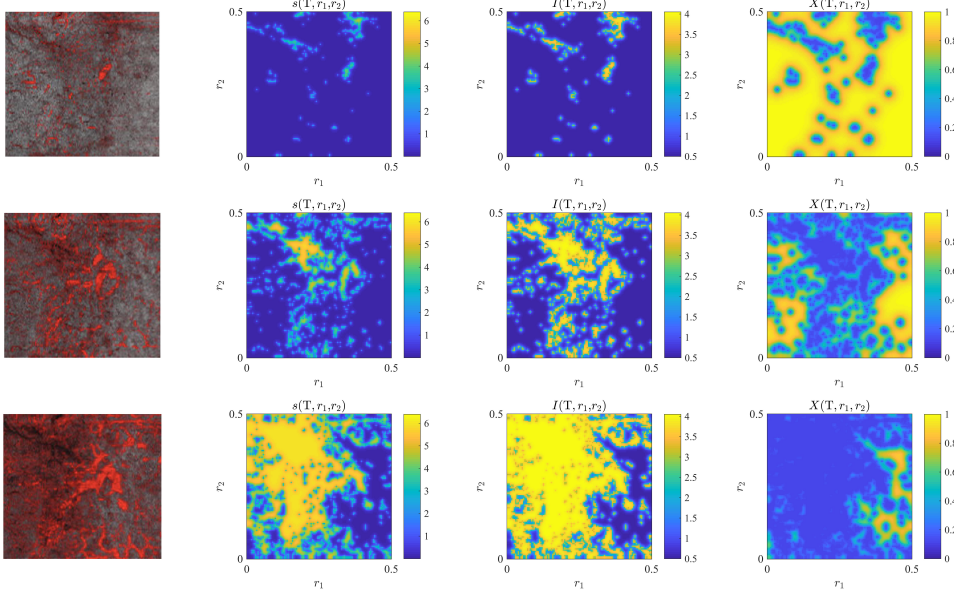


FIG. 2. First row. Plots of the oxygen concentration $s(T, \mathbf{r})$ (second panel), the cell density $I(T, \mathbf{r})$ (third panel), and the mean phenotypic state $X(T, \mathbf{r})$ (fourth panel) obtained by solving numerically the problem given by (2.3) and (2.9) subject to the initial conditions (4.5), with the set ω reconstructed from the blood vessel distribution provided by the clinical image displayed in the first panel, where the intratumor vascular network is highlighted in red, and with the parameter values listed in Table 1 except for $\eta_s = 2 \times 10^{-10} \text{ g cell}^{-1}$. Second and third rows. Same as the first row but for a different clinical image. Clinical images are taken from [82, Figure 5(d-f)] under Creative Commons licence <https://creativecommons.org/licenses/by-nc/4.0/>. These images correspond to three cross sections of a malignant melanoma at a depth of 0.02 cm (first row), 0.03 cm (second row) and 0.04 cm (third row) from the surface of the epidermis. The oxygen concentration $s(T, \mathbf{r})$ is in units of $10^{-7} \text{ g cm}^{-2}$, the cell density $I(T, \mathbf{r})$ is in units of $10^8 \text{ cells cm}^{-2}$, and the spatial variables r_1 and r_2 are in units of cm.

4.4. Numerical solutions to assess the impact of tumor tissue vascularization on intratumor phenotypic heterogeneity. In order to systematically assess the impact of tumor tissue vascularization on the level of intratumor phenotypic heterogeneity, we carry out numerical simulations considering first increasing numbers of regularly distributed blood vessels, which correspond to increasing values of the vascular density ϱ defined as

$$(4.7) \quad \varrho := \frac{|\omega|}{|\Omega|},$$

and then different random distributions of blood vessels characterized by increasing levels of vessel clustering for a fixed vascular density. We quantify the level of intratumor phenotypic heterogeneity through the following continuum versions of the equitability index $E(t)$ (defined as a rescaled Shannon diversity index) and the Simpson diversity index $D(t)$ [86, 87]

$$(4.8) \quad E(t) := - \int_0^1 \frac{F(t, x) \log F(t, x)}{\log N(t)} dx \quad \text{and} \quad D(t) := \left(\int_0^1 F^2(t, x) dx \right)^{-1},$$

where the total cell number $N(t)$ and the fraction $F(t, x)$ of cells in the phenotypic state x within the tumor are defined according to (2.2).

The results obtained varying the vascular density ϱ are summarized by the plots in Figure 3, which display the equitability index and the Simpson diversity index at the end of numerical simulations as functions of ϱ . Both diversity indices are relatively

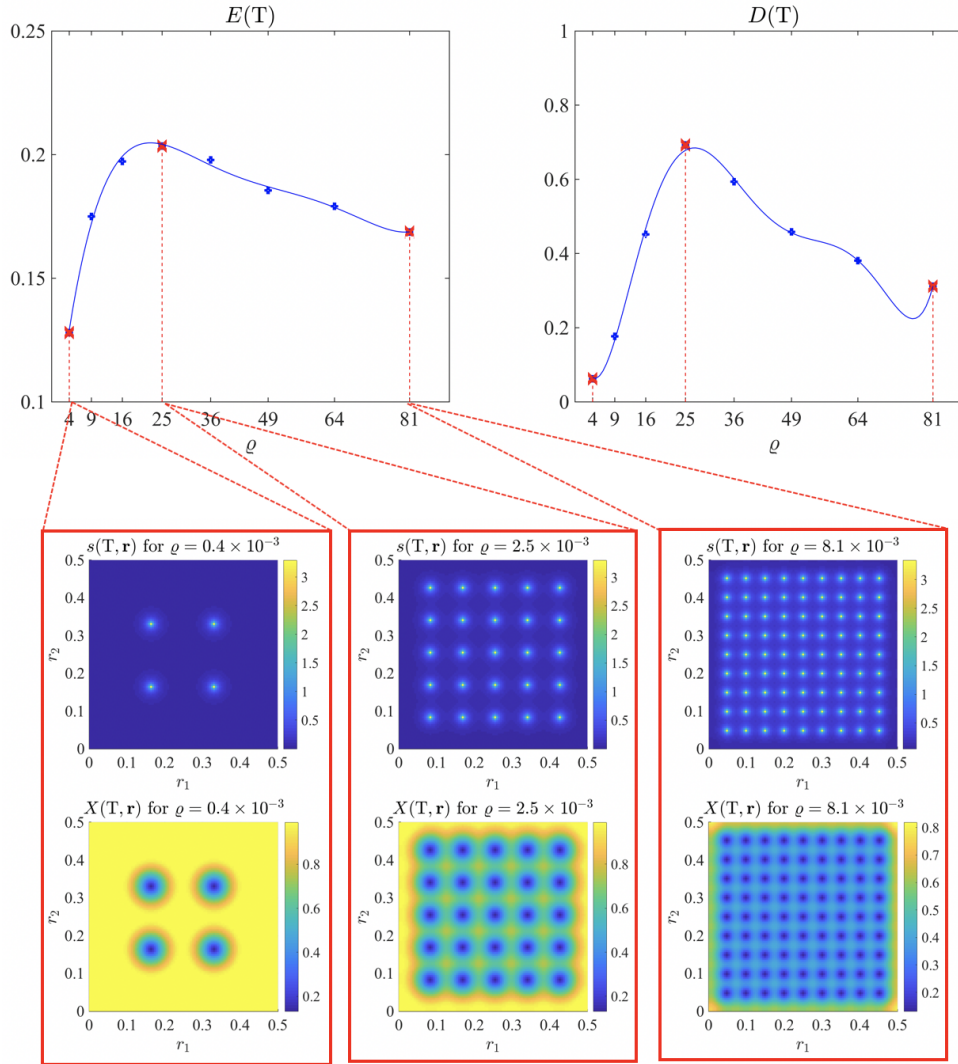


FIG. 3. Plots of the equitability index $E(T)$ and the Simpson diversity index $D(T)$ for different definitions of the set ω characterized by different values of the vascular density ϱ defined according to (4.7). The equitability index and the Simpson diversity index are computed numerically through formulas (4.8) using the numerical solutions of the problem given by (2.3) and (2.9) subject to the initial conditions (4.5), with the parameter values listed in Table 1. The insets display sample plots of the oxygen distributions $s(T, r)$ (top panel) and the mean phenotypic state $X(T, r)$ (bottom panel) corresponding to different values of ϱ . The Simpson diversity index $D(T)$ is in units of 10^4 , the vascular density ϱ is in units of 10^{-4} , the oxygen concentration $s(T, r)$ is in units of $10^{-7} \text{ g cm}^{-2}$, and the spatial variables r_1 and r_2 are in units of cm.

low for small values of the vascular density, increase and reach a maximum value for intermediate values of the vascular density—notice that both $E(T)$ and $D(T)$ attain their maximum at the same value of ϱ —and then decrease again for high values of the vascular density. This is due to the fact that, as shown by the insets in Figure 3, for low blood vessel densities the oxygen concentration $s(T, \mathbf{r})$ is uniformly low throughout Ω and, therefore, the mean phenotypic state $X(T, \mathbf{r})$ is uniformly close to $x = 1$ (cf. the insets related to $\varrho = 0.4 \times 10^{-3}$); for intermediate blood vessel densities the oxygen concentration is more heterogeneously distributed and, as a consequence, the mean phenotypic state is more diverse (cf. the insets related to $\varrho = 2.5 \times 10^{-3}$); for high blood vessel densities the oxygen concentration is relatively high throughout the tumor tissue and the mean phenotypic state is on average close to $x = 0$ (cf. the insets related to $\varrho = 8.1 \times 10^{-3}$).

The results obtained varying the level of blood vessel clustering for a fixed vascular density ϱ are summarized by the plots in Figure 4, which display the oxygen distribution $s(T, \mathbf{r})$ and the mean phenotypic state $X(T, \mathbf{r})$, along with the corresponding fraction of cells in each phenotypic state $F(T, x)$ and diversity indices $E(T)$ and $D(T)$. These results refer to an intermediate value of ϱ that corresponds to the maximum of the equitability index and the Simpson diversity index displayed in Figure 3 (i.e., $\varrho = 25 \times 10^{-4}$). Both diversity indices decrease as the level of blood vessel clustering increases (cf. the values of $E(T)$ and $D(T)$ in the insets of the panels in the third column of Figure 4). In fact, for lower levels of blood vessel clustering the oxygen concentration $s(T, \mathbf{r})$ is more heterogeneously distributed and, as a consequence, the mean phenotypic state $X(T, \mathbf{r})$ is more diverse and the cell phenotypic distribution across Ω given by $F(T, x)$ is rather uniform (cf. the plots in the first row of Figure 4). On the other hand, for higher levels of blood vessel clustering, the oxygen concentration is relatively high in the regions in close proximity to the clusters of blood vessels and relatively low throughout the rest of tumor tissue. As a result, the mean phenotypic state is mostly close to $x = 1$ with the exception of the regions near the clusters of blood vessels where it is close to $x = 0$, and the cell phenotypic distribution across the whole tumor is approximatively bimodal, with a high peak at $x = 1$ and a low peak at $x = 0$ (cf. the plots in the third row of Figure 4).

5. Conclusions and research perspectives. Intratumor phenotypic heterogeneity poses a major obstacle to anti-cancer therapy [18, 23, 42, 60, 69, 85]. It has been hypothesized that the emergence of phenotypic heterogeneity among cancer cells within malignant tumors is an eco-evolutionary process driven by spatial variability in the distribution of abiotic factors, which supports the creation of distinct ecological niches whereby cells with different phenotypic characteristics can be selected [3, 53, 68, 92]. In particular, oxygen is one of the key abiotic components of the tumor microenvironment that are implicated in the emergence of intratumor phenotypic heterogeneity [42, 64, 92].

In this paper, we have undertaken a mathematical study of the eco-evolutionary dynamics of tumor cells within vascularized tumors. Our study is based on formal asymptotic analysis and numerical simulations of a nonlocal PDE model that describes the phenotypic evolution of tumor cells and their nonlinear dynamic interactions with the oxygen, which is released from the intratumoral vascular network.

Our formal analytical results recapitulate the outcomes of previous theoretical and experimental studies on intratumor phenotypic heterogeneity [5, 35, 42, 49] by providing a mathematical formalization of the idea that local variations in the oxygen concentration bring about local variations in the phenotypic fitness landscape of the

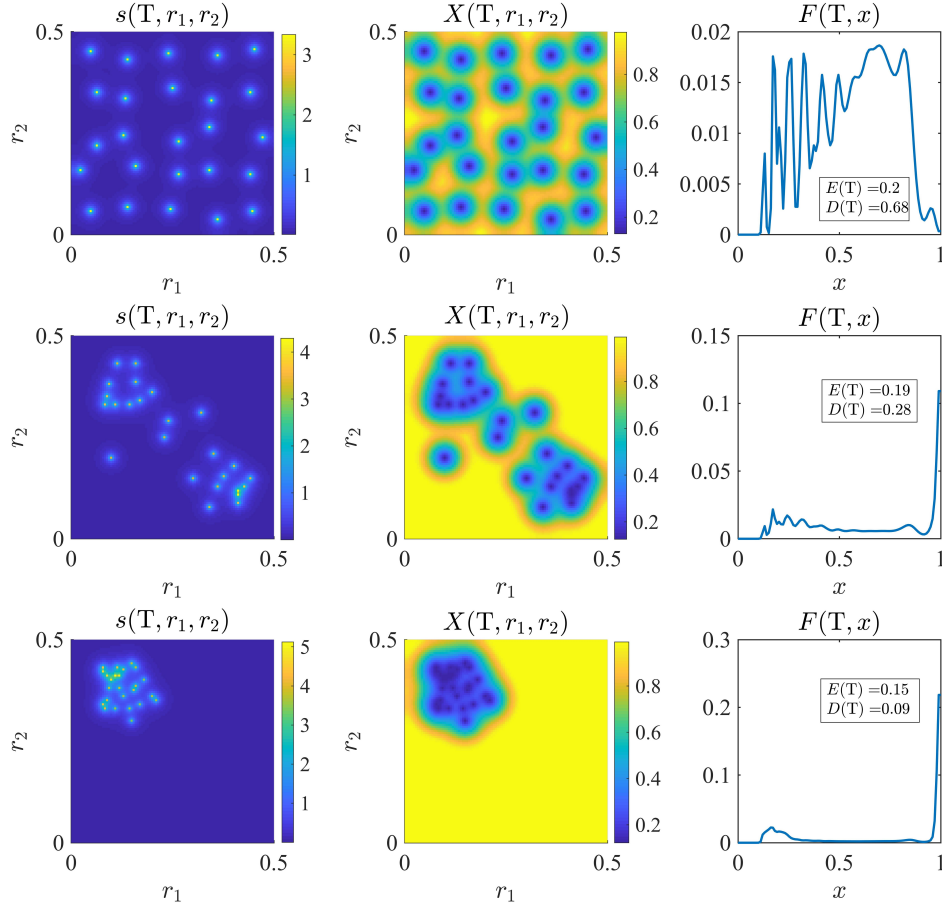


FIG. 4. First row. Plots of the oxygen distribution $s(T, \mathbf{r})$ (first panel), mean phenotypic state $X(T, \mathbf{r})$ (second panel), and fraction of cells in each phenotypic state $F(T, x)$ defined via (2.2) (third panel), for a definition of the set ω corresponding to a random distribution of blood vessels characterized by vascular density $\varrho = 25 \times 10^{-4}$ and a low level of blood vessel clustering. The values of the corresponding equitability index $E(T)$ and Simpson diversity index $D(T)$, which are computed numerically through formulas (4.8), are provided in the inset of the third panel. Second and third rows. Same as the first row but for a definition of the set ω corresponding to an intermediate level (second row) and a high level (third row) of blood vessel clustering. The oxygen concentration $s(T, \mathbf{r})$ is in units of $10^{-7} \text{ g cm}^{-2}$, the spatial variables r_1 and r_2 are in units of cm, and the Simpson diversity index $D(T)$ is in units of 10^4 .

tumor, which ultimately result in a heterogeneous intratumor phenotypic composition. Numerical simulations of the model corroborate this conclusion and show that local variations in the oxygen concentration, which are orchestrated by nonlinear dynamic interactions between tumor cells and oxygen, promote the selection of cells in different phenotypic states within the tumor depending on the distance from the blood vessels. In particular, our results offer a theoretical basis for the biological evidence that regions of the tumor tissue in the vicinity of blood vessels are densely populated by proliferative phenotypic variants, while poorly oxygenated regions are sparsely populated by hypoxic phenotypic variants [75, 84, 92, 93].

Furthermore, the results of numerical simulations of the model establish a relation between the degree of tissue vascularization and the level of intratumor phenotypic heterogeneity, measured either as the equitability index or the Simpson diversity index. This supports the idea that maps of the intratumor vascular network, which can be reconstructed from clinical images obtained via noninvasive imagine techniques, such as D-OCT [56, 82] and many others [6, 34, 44, 72, 75], could be clinically relevant, as they could be used to inform targeted anti-cancer therapy [68, 79, 80, 94].

Whilst we carried out numerical simulations considering a region of tumor tissue of area $2.5 \times 10^{-3} \text{ cm}^2$, which was chosen in agreement with clinical images provided in [82], and using parameter values that are derived from specific cancer data sets, given the robustness and structural stability of the results of formal asymptotic analysis presented here, we expect the conclusions of this study about the emergence of substantial intratumor phenotypic heterogeneity driven by eco-evolutionary processes at the cellular scale to hold when larger tumor regions and different cancer data sets are considered.

We conclude with a brief overview of possible research directions. In order to disentangle and quantify the impact of different evolutionary parameters on the emergence and development of intratumor phenotypic heterogeneity, it would be useful to have exact solutions of (2.3) in the case where the intratumor phenotypic fitness landscape is defined according to (2.4) and (4.2). This could be done by generalizing the method developed in [4, 21, 63] to construct exact solutions of nonlocal parabolic PDEs modeling the dynamics of well-mixed phenotype-structured populations to the case where spatial structure is included.

In addition, along the lines of [83], further investigations on a possible link between the topology of tumor vasculature and the level of intratumor phenotypic heterogeneity could be undertaken. Moreover, building upon the ideas presented in [8, 9], it would be interesting to study the effect on the evolutionary dynamics of tumor cells of fluctuations in the rate of oxygen inflow, which are known to influence intratumor phenotypic heterogeneity [40, 68, 81]. It would also be interesting to include the effect of temporal changes in the spatial distribution of intratumoral blood vessels, which would make it possible to explore the influence of angiogenesis on the eco-evolutionary dynamics of tumor cells in vascularized tumors. In this regard, it is a known fact that cancer cells in hypoxic conditions produce and secrete proangiogenic factors which induce the formation of new blood vessels departing from existing ones.

While the focus of this work has been on the impact of spatial variability in the oxygen concentration on the emergence of intratumor phenotypic heterogeneity, building on [31], it would be interesting to extend the modeling framework used here to incorporate the effect of nonlinear dynamic interactions between tumor cells and other abiotic factors, such as glucose and lactate, that are known to influence the levels of intratumor phenotypic heterogeneity [36, 37, 41, 53, 67, 71, 81, 100].

Furthermore, although well suited to modeling the dynamics of large cell populations, PDE models like that considered here cannot capture adaptive phenomena that are driven by stochasticity in the evolutionary paths of single cells. Therefore, it would also be interesting to complement the results of our study with numerical simulations of corresponding individual-based models which track the evolutionary trajectories of single cells across a space of discrete phenotypic states, as similarly done in [7, 21, 23, 89]. This would make it possible to have a more precise description of the phenotypic evolution of tumor cells in cases where cell numbers are relatively low and, therefore, stochastic fluctuations in single-cell phenotypic properties will have a stronger impact on intratumor phenotypic heterogeneity.

Finally, we plan to extend the model considered here to carry out a mathematical study of the eco-evolutionary dynamics of tumor cells in metastatic tumors. In this respect, a modeling approach analogous to the one presented in [33], whereby different metastatic sites are represented as distinct compartments and the metastatization process is modeled by allowing tumor cells to transition from one site to another through the intratumor blood vessels seen as entry/exit locations, may prove useful.

REFERENCES

- [1] M. ALFARO, H. BERESTYCKI, AND G. RAOUL, *The effect of climate shift on a species submitted to dispersion, evolution, growth, and nonlocal competition*, SIAM J. Math. Anal., 49 (2017), pp. 562–596.
- [2] M. ALFARO, J. COVILLE, AND G. RAOUL, *Travelling waves in a nonlocal reaction-diffusion equation as a model for a population structured by a space variable and a phenotypic trait*, Comm. Partial Differential Equations, 38 (2013), pp. 2126–2154.
- [3] K. O. ALFAROUK, M. E. IBRAHIM, R. A. GATENBY, AND J. S. BROWN, *Riparian ecosystems in human cancers*, Evolutionary Appl., 6 (2013), pp. 46–53.
- [4] L. ALMEIDA, P. BAGNERINI, G. FABRINI, B. D. HUGHES, AND T. LORENZI, *Evolution of cancer cell populations under cytotoxic therapy and treatment optimisation: Insight from a phenotype-structured mode*, ESAIM Math. Model. Numer. Anal., 53 (2019), pp. 1157–1190.
- [5] A. R. ANDERSON, A. M. WEAVER, P. T. CUMMINGS, AND V. QUARANTA, *Tumor morphology and phenotypic evolution driven by selective pressure from the microenvironment*, Cell, 127 (2006), pp. 905–915.
- [6] H. ANDERSON, P. PRICE, M. BLOMLEY, M. LEACH, AND P. WORKMAN, *Measuring changes in human tumour vasculature in response to therapy using functional imaging techniques*, Br. J. Cancer, 85 (2001), pp. 1085–1093.
- [7] A. ARDAŠEVA, R. A. GATENBY, A. R. ANDERSON, H. M. BYRNE, P. K. MAINI, AND T. LORENZI, *A comparative study between discrete and continuum models for the evolution of competing phenotype-structured cell populations in dynamical environments*, Phys. Rev. E, in process.
- [8] A. ARDAŠEVA, R. A. GATENBY, A. R. ANDERSON, H. M. BYRNE, P. K. MAINI, AND T. LORENZI, *Evolutionary dynamics of competing phenotype-structured populations in periodically fluctuating environments*, J. Math. Biol., 80 (2020), pp. 775–807.
- [9] A. ARDAŠEVA, R. A. GATENBY, A. R. ANDERSON, H. M. BYRNE, P. K. MAINI, AND T. LORENZI, *A mathematical dissection of the adaptation of cell populations to fluctuating oxygen levels*, Bull. Math. Biol., 82 (2020), p. 81, <https://doi.org/10.1007/s11538-020-00754-7>.
- [10] A. ARNOLD, L. DESVILLETTES, AND C. PRÉVOST, *Existence of nontrivial steady states for populations structured with respect to space and a continuous trait*, Comm. Pure Appl. Anal., 11 (2012), pp. 83–96.
- [11] G. BARLES, L. C. EVANS, AND P. E. SOUGANIDIS, *Wavefront propagation for reaction-diffusion systems of PDE*, Duke Math. J., 61 (1989), pp. 835–858.
- [12] G. BARLES, S. MIRRAHIMI, B. PERTHAME, ET AL., *Concentration in Lotka-Volterra parabolic or integral equations: A general convergence result*, Methods Appl. Anal., 16 (2009), pp. 321–340.
- [13] E. BOUIN AND V. CALVEZ, *Travelling waves for the cane toads equation with bounded traits*, Nonlinearity, 27 (2014), p. 2233.
- [14] E. BOUIN, V. CALVEZ, N. MEUNIER, S. MIRRAHIMI, B. PERTHAME, G. RAOUL, AND R. VOTURIEZ, *Invasion fronts with variable motility: Phenotype selection, spatial sorting and wave acceleration*, C. R. Math., 350 (2012), pp. 761–766.
- [15] E. BOUIN AND S. MIRRAHIMI, *A Hamilton-Jacobi approach for a model of population structured by space and trait*, Comm. Math. Sci., 13 (2015), pp. 1431–1452.
- [16] J. M. BROWN AND A. J. GIACCIA, *The unique physiology of solid tumors: Opportunities (and problems) for cancer therapy*, Cancer Res., 58 (1998), pp. 1408–1416.
- [17] J. M. BROWN AND W. R. WILSON, *Exploiting tumour hypoxia in cancer treatment*, Nature Rev. Cancer, 4 (2004), p. 437.
- [18] R. A. BURRELL AND C. SWANTON, *Tumour heterogeneity and the evolution of polyclonal drug resistance*, Molecular Oncology, 8 (2014), pp. 1095–1111.

- [19] V. CALVEZ, C. HENDERSON, S. MIRRAHIMI, O. TURANOVA, AND T. DUMONT, *Non-local Competition Slows Down Front Acceleration During Dispersal Evolution*, preprint, arXiv:1810.07634, 2018.
- [20] J. J. CASCIARI, S. V. SOTIRCHOS, AND R. M. SUTHERLAND, *Variations in tumor cell growth rates and metabolism with oxygen concentration, glucose concentration, and extracellular pH*, *J. Cellular Physiology*, 151 (1992), pp. 386–394.
- [21] R. H. CHISHOLM, T. LORENZI, L. DESVILLETTES, AND B. D. HUGHES, *Evolutionary dynamics of phenotype-structured populations: From individual-level mechanisms to population-level consequences*, *Zeitschrift für Angewandte Mathematik und Physik*, 67 (2016), p. 100.
- [22] R. H. CHISHOLM, T. LORENZI, AND A. LORZ, *Effects of an advection term in nonlocal Lotka–Volterra equations*, *Comm. Math. Sci.*, 14 (2016), pp. 1181–1188.
- [23] R. H. CHISHOLM, T. LORENZI, A. LORZ, A. K. LARSEN, L. ALMEIDA, A. ESCARGUEIL, AND J. CLAIRAMBault, *Emergence of drug tolerance in cancer cell populations: An evolutionary outcome of selection, non-genetic instability and stress-induced adaptation*, *Cancer Res.*, 75 (2015), pp. 930–939.
- [24] P. CUMSILLE, A. CORONEL, C. CONCA, C. QUIÑINAO, AND C. ESCUDERO, *Proposal of a hybrid approach for tumor progression and tumor-induced angiogenesis*, *Theoret. Biol. Med. Model.*, 12 (2015), p. 13.
- [25] L. DESVILLETTES, P.-E. JABIN, S. MISCHLER, G. RAOUL, ET AL., *On selection dynamics for continuous structured populations*, *Comm. Math. Sci.*, 6 (2008), pp. 729–747.
- [26] O. DIEKMANN, P.-E. JABIN, S. MISCHLER, AND B. PERTHAME, *The dynamics of adaptation: An illuminating example and a Hamilton–Jacobi approach*, *Theoret. Pop. Biol.*, 67 (2005), pp. 257–271.
- [27] W. DOERFLER AND P. BÖHM, *DNA Methylation: Development, Genetic Disease and Cancer*, vol. 310, Springer Science & Business Media, New York, 2006.
- [28] P. DOMSCHKE, D. TRUCU, A. GERISCH, AND M. A. CHAPLAIN, *Structured models of cell migration incorporating molecular binding processes*, *J. Math. Biol.*, 75 (2017), pp. 1517–1561.
- [29] P. DUESBERG, R. STINDL, AND R. HEHLMANN, *Explaining the high mutation rates of cancer cells to drug and multidrug resistance by chromosome reassortments that are catalyzed by aneuploidy*, *Proc. Nat. Acad. Sci.*, 97 (2000), pp. 14295–14300.
- [30] L. C. EVANS AND P. E. SOUGANIDIS, *A PDE approach to geometric optics for certain semi-linear parabolic equations*, *Indiana Univ. Math. J.*, 38 (1989), pp. 141–172.
- [31] G. FIANDACA, M. DELITALA, AND T. LORENZI, *A Mathematical Study of the Influence of Hypoxia and Acidity on the Evolutionary Dynamics of Cancer*, preprint, arXiv:2009.00251, 2020.
- [32] W. H. FLEMING AND P. E. SOUGANIDIS, *PDE-viscosity solution approach to some problems of large deviations*, *Annali della Scuola Normale Superiore di Pisa-Classe di Scienze*, 13 (1986), pp. 171–192.
- [33] L. C. FRANSSEN, T. LORENZI, A. E. BURGESS, AND M. A. CHAPLAIN, *A mathematical framework for modelling the metastatic spread of cancer*, *Bull. Math. Biol.*, 81 (2019), pp. 1965–2010.
- [34] D. FUKUMURA, D. G. DUDA, L. L. MUNN, AND R. K. JAIN, *Tumor microvasculature and microenvironment: Novel insights through intravital imaging in pre-clinical models*, *Micrcirculation*, 17 (2010), pp. 206–225.
- [35] J. GALLAHER AND A. R. ANDERSON, *Evolution of intratumoral phenotypic heterogeneity: The role of trait inheritance*, *Interface Focus*, 3 (2013), p. 20130016.
- [36] R. GATENBY, K. SMALLBONE, P. MAINI, F. ROSE, J. AVERILL, R. NAGLE, L. WORRALL, AND R. GILLIES, *Cellular adaptations to hypoxia and acidosis during somatic evolution of breast cancer*, *British J. Cancer*, 97 (2007), p. 646.
- [37] R. A. GATENBY AND R. J. GILLIES, *Glycolysis in cancer: A potential target for therapy*, *The Int. J. Biochem. & Cell Biol.*, 39 (2007), pp. 1358–1366.
- [38] L. GAY, A.-M. BAKER, AND T. A. GRAHAM, *Tumour cell heterogeneity*, *F1000Research*, 5 (2016), p. 238.
- [39] A. GIATROMANOLAKI, M. KOUKOURAKIS, E. SIVRIDIS, H. TURLEY, K. TALKS, F. PEZZELLA, K. GATTER, AND A. HARRIS, *Relation of hypoxia inducible factor 1 α and 2 α in operable non-small cell lung cancer to angiogenic/molecular profile of tumours and survival*, *British J. Cancer*, 85 (2001), p. 881.
- [40] R. J. GILLIES, J. S. BROWN, A. R. ANDERSON, AND R. A. GATENBY, *Eco-evolutionary causes and consequences of temporal changes in intratumoural blood flow*, *Nature Rev. Cancer*, (2018), p. 1.

- [41] R. J. GILLIES AND R. A. GATENBY, *Hypoxia and adaptive landscapes in the evolution of carcinogenesis*, Cancer Metastasis Rev., 26 (2007), pp. 311–317.
- [42] R. J. GILLIES, D. VERDUZCO, AND R. A. GATENBY, *Evolutionary dynamics of carcinogenesis and why targeted therapy does not work*, Nature Rev. Cancer, 12 (2012), p. 487.
- [43] J. D. GORDAN, J. A. BERTOUT, C.-J. HU, J. A. DIEHL, AND M. C. SIMON, *HIF-2 α promotes hypoxic cell proliferation by enhancing c-myc transcriptional activity*, Cancer Cell, 11 (2007), pp. 335–347.
- [44] D. R. GRIMES, P. KANNAN, D. R. WARREN, B. MARKELC, R. BATES, R. MUSCHEL, AND M. PARTRIDGE, *Estimating oxygen distribution from vasculature in three-dimensional tumour tissue*, J. Roy. Soc. Interface, 13 (2016), 20160070.
- [45] L. HLATKY AND E. ALPEN, *Two-dimensional diffusion limited system for cell growth*, Cell Proliferation, 18 (1985), pp. 597–611.
- [46] M. HOCKEL AND P. VAUPEL, *Tumor hypoxia: Definitions and current clinical, biologic, and molecular aspects*, J. Nat. Cancer Inst., 93 (2001), pp. 266–276.
- [47] A. HODGKINSON, G. UZÉ, O. RADULESCU, AND D. TRUCU, *Signal propagation in sensing and reciprocating cellular systems with spatial and structural heterogeneity*, Bull. Math. Biol., 80 (2018), pp. 1900–1936.
- [48] S. HUANG, *Genetic and non-genetic instability in tumor progression: Link between the fitness landscape and the epigenetic landscape of cancer cells*, Cancer Metastasis Rev., 32 (2013), pp. 423–448.
- [49] A. IBRAHIM-HASHIM, M. ROBERTSON-TESSI, P. ENRIZUES-NAVAS, M. DAMAGHI, Y. BALAGURUNATHAN, J. W. WOJTKOWIAK, S. RUSSELL, K. YOONSEOK, M. C. LLOYD, M. M. BUI, ET AL., *Defining cancer subpopulations by adaptive strategies rather than molecular properties provides novel insights into intratumoral evolution*, Cancer Res., 77 (2017), pp. 2242–2254.
- [50] P.-E. JABIN AND R. S. SCHRAM, *Selection-mutation Dynamics with Spatial Dependence*, preprint, arXiv:1601.04553, 2016.
- [51] R. K. JAIN, *Determinants of tumor blood flow: A review*, Cancer Res., 48 (1988), pp. 2641–2658.
- [52] B. F. JORDAN AND P. SONVEAUX, *Targeting tumor perfusion and oxygenation to improve the outcome of anticancer therapy*, Frontiers in Pharmacology, 3 (2012), p. 94.
- [53] A. KAZNATCHEEV, R. VANDER VELDE, J. G. SCOTT, AND D. BASANTA, *Cancer treatment scheduling and dynamic heterogeneity in social dilemmas of tumour acidity and vasculature*, British J. Cancer, 116 (2017), p. 785.
- [54] L. S. KUMOSA, T. L. ROUTH, J. T. LIN, J. Y. LUCISANO, AND D. A. GOUGH, *Permeability of subcutaneous tissues surrounding long-term implants to oxygen*, Biomaterials, 35 (2014), pp. 8287–8296.
- [55] R. LANDE AND S. J. ARNOLD, *The measurement of selection on correlated characters*, Evolution, 37 (1983), pp. 1210–1226.
- [56] B. LAVIÑA, *Brain vascular imaging techniques*, Int. J. Molecular Sci., 18 (2016), p. 70.
- [57] J.-W. LEE, S.-H. BAE, J.-W. JEONG, S.-H. KIM, AND K.-W. KIM, *Hypoxia-inducible factor (HIF-1) α : Its protein stability and biological functions*, Experimental & Molecular Medicine, 36 (2004), p. 1.
- [58] R. J. LEVEQUE, *Finite Difference Methods for Ordinary and Partial Differential Equations: Steady-state and Time-dependent Problems*, SIAM, Philadelphia, 2007.
- [59] C. K. LI, *The glucose distribution in 9l rat brain multicell tumor spheroids and its effect on cell necrosis*, Cancer, 50 (1982), pp. 2066–2073.
- [60] K. A. LIPINSKI, L. J. BARBER, M. N. DAVIES, M. ASHENDEN, A. SOTTORIVA, AND M. GERLINGER, *Cancer evolution and the limits of predictability in precision cancer medicine*, Trends in Cancer, 2 (2016), pp. 49–63.
- [61] M. C. LLOYD, J. J. CUNNINGHAM, M. M. BUI, R. J. GILLIES, J. S. BROWN, AND R. A. GATENBY, *Darwinian dynamics of intratumoral heterogeneity: Not solely random mutations but also variable environmental selection forces*, Cancer Res., 76 (2016), pp. 3136–3144.
- [62] L. A. LOEB, *A mutator phenotype in cancer*, Cancer Res., 61 (2001), pp. 3230–3239.
- [63] T. LORENZI, R. H. CHISHOLM, AND J. CLAIRAMBAULT, *Tracking the evolution of cancer cell populations through the mathematical lens of phenotype-structured equations*, Biology Direct, 11 (2016), p. 43.
- [64] T. LORENZI, C. VENKATARAMAN, A. LORZ, AND M. A. CHAPLAIN, *The role of spatial variations of abiotic factors in mediating intratumour phenotypic heterogeneity*, J. Theoret. Biol., 451 (2018), pp. 101–110.

- [65] A. LORZ, T. LORENZI, J. CLAIRAMBAULT, A. ESCARGUEIL, AND B. PERTHAME, *Modeling the effects of space structure and combination therapies on phenotypic heterogeneity and drug resistance in solid tumors*, Bull. Math. Biol., 77 (2015), pp. 1–22.
- [66] A. LORZ, S. MIRRAHIMI, AND B. PERTHAME, *Dirac mass dynamics in multidimensional non-local parabolic equations*, Comm. Partial Differential Equations, 36 (2011), pp. 1071–1098.
- [67] V. S. MANEM, K. KAVEH, M. KOHANDEL, AND S. SIVALOGANATHAN, *Modeling invasion dynamics with spatial random-fitness due to micro-environment*, PloS One, 10 (2015), e0140234.
- [68] A. MARUSYK, V. ALMENDRO, AND K. POLYAK, *Intra-tumour heterogeneity: A looking glass for cancer?*, Nature Rev. Cancer, 12 (2012), p. 323.
- [69] F. MICHOR AND K. POLYAK, *The origins and implications of intratumor heterogeneity*, Cancer Prevention Res., 3 (2010), pp. 1361–1364.
- [70] S. MIRRAHIMI AND B. PERTHAME, *Asymptotic analysis of a selection model with space*, J. Math. Pures Appl., 104 (2015), pp. 1108–1118.
- [71] H. R. MOLAVIAN, M. KOHANDEL, M. MILOSEVIC, AND S. SIVALOGANATHAN, *Fingerprint of cell metabolism in the experimentally observed interstitial ph and po₂ in solid tumors*, Cancer Res., 69 (2009), pp. 9141–9147.
- [72] A. R. NOBRE, D. ENTENBERG, Y. WANG, J. CONDEELIS, AND J. A. AGUIRRE-GHISO, *The different routes to metastasis via hypoxia-regulated programs*, Trends in Cell Biology, 28 (2018), pp. 941–956.
- [73] J. OLSEN, J. HOLMES, AND G. B. JEMEC, *Advances in optical coherence tomography in dermatology—a review*, J. Biomedical Optics, 23 (2018), 040901.
- [74] J. OTWINOWSKI AND J. B. PLOTKIN, *Inferring fitness landscapes by regression produces biased estimates of epistasis*, Proc. Nat. Acad. Sci., 111 (2014), pp. E2301–E2309.
- [75] A. R. PADHANI, K. A. KROHN, J. S. LEWIS, AND M. ALBER, *Imaging oxygenation of human tumours*, European Radiology, 17 (2007), pp. 861–872.
- [76] B. PERTHAME, *Transport Equations in Biology*, Springer Science & Business Media, New York, 2006.
- [77] B. PERTHAME AND G. BARLES, *Dirac concentrations in Lotka-Volterra parabolic pdes*, Indiana Univ. Math. J., 57 (2008), pp. 3275–3301.
- [78] J. POLESZCZUK, P. HAHNFELDT, AND H. ENDERLING, *Evolution and phenotypic selection of cancer stem cells*, PLoS Comput. Biol., 11 (2015), e1004025.
- [79] G. POWATHIL, M. KOHANDEL, M. MILOSEVIC, AND S. SIVALOGANATHAN, *Modeling the spatial distribution of chronic tumor hypoxia: Implications for experimental and clinical studies*, Comput. Math. Methods Med., 2012 (2012), 410602.
- [80] G. G. POWATHIL, K. E. GORDON, L. A. HILL, AND M. A. CHAPLAIN, *Modelling the effects of cell-cycle heterogeneity on the response of a solid tumour to chemotherapy: Biological insights from a hybrid multiscale cellular automaton model*, J. Theoret. Biol., 308 (2012), pp. 1–19.
- [81] M. ROBERTSON-TESSI, R. J. GILLIES, R. A. GATENBY, AND A. R. ANDERSON, *Impact of metabolic heterogeneity on tumor growth, invasion, and treatment outcomes*, Cancer Res., 75 (2015), pp. 1567–1579.
- [82] S. SCHUH, J. HOLMES, M. ULRICH, L. THEMSTRUP, G. B. JEMEC, N. DE CARVALHO, G. PELLACANI, AND J. WELZEL, *Imaging blood vessel morphology in skin: Dynamic optical coherence tomography as a novel potential diagnostic tool in dermatology*, Dermatology and Therapy, 7 (2017), pp. 187–202.
- [83] J. G. SCOTT, A. G. FLETCHER, A. R. ANDERSON, AND P. K. MAINI, *Spatial metrics of tumour vascular organisation predict radiation efficacy in a computational model*, PLoS Comput. Biol., 12 (2016), e1004712.
- [84] G. L. SEMENZA, *Targeting hif-1 for cancer therapy*, Nature Rev. Cancer, 3 (2003), p. 721.
- [85] M. A. SHAH AND G. K. SCHWARTZ, *Cell cycle-mediated drug resistance: An emerging concept in cancer therapy*, Clinical Cancer Res., 7 (2001), pp. 2168–2181.
- [86] C. E. SHANNON, *A mathematical theory of communication*, Bell System Technical Journal, 27 (1948), pp. 379–423.
- [87] E. H. SIMPSON, *Measurement of diversity*, Nature, 163 (1949), p. 688.
- [88] J. T. SMITH, J. K. TOMFOHR, M. C. WELLS, T. P. BEEBE, T. B. KEPLER, AND W. M. REICHERT, *Measurement of cell migration on surface-bound fibronectin gradients*, Langmuir, 20 (2004), pp. 8279–8286.
- [89] R. E. STACE, T. STIEHL, M. A. CHAPLAIN, A. MARCINIAK-CZUCHRA, AND T. LORENZI, *Discrete and continuum phenotype-structured models for the evolution of cancer cell populations under chemotherapy*, Math. Model. Natural Phenomena, 15 (2020), p. 14.
- [90] J. R. STINCHCOMBE, A. F. AGRAWAL, P. A. HOHENLOHE, S. J. ARNOLD, AND M. W. BLOWS, *Estimating nonlinear selection gradients using quadratic regression coefficients: Double or nothing?*, Evolution: Int. J. Organic Evolution, 62 (2008), pp. 2435–2440.

- [91] S. STRESE, M. FRYKNÄS, R. LARSSON, AND J. GULLBO, *Effects of hypoxia on human cancer cell line chemosensitivity*, BMC Cancer, 13 (2013), p. 331.
- [92] X.-X. SUN AND Q. YU, *Intra-tumor heterogeneity of cancer cells and its implications for cancer treatment*, Acta Pharmacologica Sinica, 36 (2015), p. 1219.
- [93] I. TANNOCK, *The relation between cell proliferation and the vascular system in a transplanted mouse mammary tumour*, British J. Cancer, 22 (1968), p. 258.
- [94] P. VAUPEL, *Tumor microenvironmental physiology and its implications for radiation oncology*, Seminars in Radiation Oncology, 14 (2004), pp. 198–206.
- [95] P. VAUPEL, F. KALLINOWSKI, AND P. OKUNIEFF, *Blood flow, oxygen and nutrient supply, and metabolic microenvironment of human tumors: A review*, Cancer Res., 49 (1989), pp. 6449–6465.
- [96] S. E. WANG, P. HINOW, N. BRYCE, A. M. WEAVER, L. ESTRADA, C. L. ARTEAGA, AND G. F. WEBB, *A mathematical model quantifies proliferation and motility effects of TGF- β on cancer cells*, Comput. Math. Methods Med., 10 (2009), pp. 71–83.
- [97] J. P. WARD AND J. KING, *Mathematical modelling of avascular-tumour growth*, Math. Med. Biol., 14 (1997), pp. 39–69.
- [98] T. XIA, H. CHENG, AND Y. ZHU, *Knockdown of hypoxia-inducible factor-1 alpha reduces proliferation, induces apoptosis and attenuates the aggressive phenotype of retinoblastoma *weki-RB-1* cells under hypoxic conditions*, Ann. Clinical Lab. Sci., 44 (2014), pp. 134–144.
- [99] T. A. YAP, M. GERLINGER, P. A. FUTREAL, L. PUSZTAI, AND C. SWANTON, *Intratumor heterogeneity: Seeing the wood for the trees*, Sci. Translational Med., 4 (2012), pp. 127ps10–127ps10.
- [100] Y. ZHAO, E. B. BUTLER, AND M. TAN, *Targeting cellular metabolism to improve cancer therapeutics*, Cell Death & Disease, 4 (2013), p. e532.